Journal of the Brazilian Society of Mechanical Sciences and Engineering (2020) 42:480
https://doi.org/10.1007/s40430-020-02567-0

TECHNICAL PAPER

A study on wire and arc additive manufacturing of low-carbon steel components: process stability, microstructural and mechanical properties

Van Thao Le[1,2] · Dinh Si Mai[2] · Quang Huy Hoang[2]

Received: 28 April 2020 / Accepted: 13 August 2020

Abstract
Among metal-based additive manufacturing, wire and arc additive manufacturing is receiving increasing attention for the production of components with medium to large dimensions. In the current research, the production of low-carbon steel thin-walled components by wire and arc additive manufacturing was addressed. Firstly, the influence of two depositing direction strategies on the wall shape was investigated. Subsequently, the effect of heat input on the shape stability and the microstructure evolution of the walls was studied. The results indicated that the alternating depositing direction strategy was more suited to build thin walls with relatively regular height. The heat input significantly influenced the shape stability, but had slight effects on the microstructure evolution. The microstructure of the walls varied from the top to the bottom regions, leading to a variation in hardness from 157 ± 3.11 to 192 ± 4.30 (HV5). The microstructure of the built thin walls can be distinguished in three regions: The upper region exhibited lamellar structures; the middle region dominantly featured granular structures of ferrites with a small proportion of pearlites, which appear in the boundaries of grains; and the lower region showed a mix of lamellar and equiaxed structures of ferrites. The tensile properties of the built material also exhibited anisotropic characteristics: The yield strength and ultimate tensile strength vary from 320 ± 6 to 362 ± 8 MPa and from 429 ± 8 to 479 ± 7 MPa, respectively.

Keywords Wire and arc additive manufacturing · Low-carbon steel · Microstructure · Mechanical properties

1 Introduction

In the last decades, additive manufacturing (AM) has emerged as a new technology for manufacturing parts with highly complex geometries, including internal structures. The AM technique allows the manufacture of a physical part directly from its CAD model without requiring extra resources, for example cutting tools, jigs, and coolant fluids as in machining [1]. Thanks to the layer-by-layer manufacturing principle, AM uses only an amount of materials required to build designed parts and support structures if necessary. Thus, the waste of materials and environmental impacts could be reduced [2, 3]. AM also enables the topological optimization for saving raw materials [4]. Nowadays, AM technologies, in particular metallic AM technologies, are effectively used in aeronautics, automobile, and biomedical engineering [1, 5].

Among metallic AM technologies, wire and arc additive manufacturing (WAAM) appears as the most beneficial technique to produce components with large dimensions. In WAAM systems, a welding source is used to make the arc between the electrode and the workpiece to melt the metallic wire. The welding source can be gas tungsten arc welding (GTAW), plasma arc welding (PAW), and gas metal arc welding (GMAW) [6, 7]. In comparison with powder bed fusion (PBF)-based AM and powder feed deposition (PFD)-based AM, WAAM exhibits a high deposition rate and low costs of investment and production [6, 7]. The deposition rate of WAAM can reach up to 4–9 kg/h, whereas that of PBF-based AM is about 50 g/h and that of PFD-based AM is roughly equal to 1 kg/h [8]. WAAM is also

Technical Editor: Lincoln Cardoso Brandao.

✉ Van Thao Le
thaomta@gmail.com

[1] Institute of Research and Development, Duy Tan University, Da Nang 550000, Vietnam

[2] Advanced Technology Center, Le Quy Don Technical University, Hanoi 100000, Vietnam

Published online: 19 August 2020

much cheaper than other metal-based AM systems, and the production of the wire feedstock is cheaper than that of the metal powder. Therefore, WAAM is a more cost-effective and suited solution for the production of large-scale components in the industry. However, the surface quality and dimensional accuracy of WAAM components are very low. The surface roughness of WAAM components is about 0.5 mm, while that of PBF- and PFD-based AM is about 20–100 µm. WAAM components also feature high thermal distortions and residual stresses. Among WAAM processes, GMAW-based AM presents a lower level of part accuracy and process stability. PAW-based AM provides the highest energy density, which allows high travel speeds and high quality of welding beads with minimized distortion. However, PAW-based AM normally requires the most expensive investment [9]. When compared with the deposition rate of GTAW- and PAW-based AM, the deposition rate of GMAW-based AM is about two times greater [10]. Hence, the GMAW-based AM process is well suited to build large-dimensional components.

Recently, the GMAW-based AM process has been extensively investigated in terms of technological performance, optimization of process parameters, and metallurgical properties [11–19]. For example, Xiong et al. [15] studied the possibility of using the GMAW-based AM process for fabricating inclined thin-walled components. Yang et al. [13] analyzed the thermal distortion of GMAW-based AM-built thin-walled components. The authors stated that the external quality of thin walls was enhanced by increasing the interpass time between two successive deposits. Residual stresses in WAAM components could also be reduced by increasing the interpass time, as demonstrated by Zhao et al. [20]. However, if more the interpass cooling times are applied, the productivity will be decreased. In terms of internal quality of manufactured components, it is essential to understand the microstructure evolution and the change in terms of mechanical properties within one component. Recently, Ortega et al. [21] used CMT (cold metal transfer) as a heat source in the GMAW-based AM process to build 4043 aluminum thin walls. The effects of traveling speed and power on the wall shape were investigated. The authors demonstrated that the increase in travel speed leads to decrease in the width of welding beads and the thin walls. Gokhale et al. [22] carried out a study, in which a set of optimized process parameters was determined to build thin-walled components by using the GTAW-based AM process. The authors pointed out that the optimized process parameters enable thin-walled components to be built with a desirable thickness and a good shape quality. However, in their work, the microstructures, hardness, and tensile strengths of the built thin-walled material were not explored.

Up to now, considerable studies on microstructure and mechanical properties of WAAM-built parts are carried out in the cases of titanium and nicked alloys, as well as aluminum alloys [23–25]. However, studies on the metallurgical characterization of GMAW-based AM-built steel parts are still limited. Low-carbon steels are widely used in different sectors, such as construction, transport, appliances and industry. In automotive industry and construction sectors, low-carbon steels are generally used in forms of strip steels and structural steels. About 50–60% weight of the vehicles was constituted by low-carbon steel [26]. Recently, WAAM technologies were also used to fabricate lightweight low-carbon/austenite stainless steel components composed of thin-walled features, for example the arm of excavators [27] (Fig. 1a), tubular components (Fig. 1b) [28], the footbridge (Fig. 1c) [29], and so on.

The microstructural and mechanical characteristics of WAAM-built medium-carbon and low-carbon steel components were investigated by a number of authors. Haden et al. [30] carried out a study in which a WAAM system was used to build thin walls from both low-carbon steel (ER70S) and 304 steel. They demonstrated that the tensile strength of both low-carbon steel and 304 steel walls produced by WAAM falls within the same value range as that of wrought low-carbon and 304 steels, respectively. Rafieazad et al. [31] used GMAW-based AM to produce multilayer multibead low-carbon steel components. These authors reported that the tensile strength

Fig. 1 Some examples of steel thin-walled components and steel components composed of thin-walled features fabricated by WAAM: **a** the excavator arm [27], **b** tubular components [28], and **c** the footbridge [29]

in the building direction and that in the welding direction were comparable. However, the ductility in the welding direction was higher than that in the building direction. Lin et al. [32] explored the metallurgical characterization of medium-carbon steel (XC-45) manufactured by WAAM. They stated that the hardness and tensile strengths of WAAM XC-45 parts are comparable to those of AISI-1045 steel fabricated by conventional manufacturing processes. The anisotropy in terms of microstructures causes the tensile strength difference between the building direction and the welding direction.

In this study, a better insight into the manufacture of thin-walled low-carbon steel components built by WAAM is addressed. The effect of two deposition strategies on the geometry of walls was firstly investigated in order to select the most suitable one. Subsequently, different levels of heat input were used to build thin walls for observing the effects of the heat input on the shape stability and the microstructure evolution of the built material. The variation in microstructures in different regions of built thin walls was also analyzed. Finally, the tensile strengths of WAAM thin walls had been investigated in order to confirm the compatibility of WAAM components with industrial applications.

2 Materials and research methodology

The 1.2-mm-diameter copper-coated ER70S-6 steel wire was used as the consumable electrode in the welding process. Its chemical composition is shown in Table 1. The ER70S-6 steel wire was selected because it is widely used in the welding field for different industrial applications, including structural steel components, auto bodies, pipes, and so on. It is also usually available in the workshops.

Two low-carbon steel (SS400) plates with dimensions of 250 × 100 × 10 mm were used as the substrates for the welding deposition. An industrial robotic gas metal arc welding system (Panasonic TA-1400) was employed to produce the thin walls upon the substrates according to the AM principle. The motions of the welding torch are performed by a six-axis robot. During the welding process, a 100% CO_2 gas was employed for the shielding purpose with a flow rate of 15 L/min. The 100% CO_2 gas was selected for the shielding purpose because it is the cheapest gas and allows producing a deep welding penetration. This gas is also commonly available in the workshops.

In the current study, to achieve different objectives as mentioned above, three following research stages were carried out as follows:

(1) Investigation on the effects of deposition strategies on the shape of built thin walls.

In the first stage, two strategies—the same deposition direction (Fig. 2a) and the alternating deposition direction (Fig. 2b)—were used for building thin-walled samples on the substrates. In the first strategy, all welding layers were deposited in the same direction (Fig. 2a). On the other hand, in the second one, the deposition directions of two adjacent layers are opposite. Namely, the starting point of a new deposition layer is placed at the ending point of the last deposition layer (Fig. 2b).

In both strategies, when a deposit was completed, the torch was moved to the starting point of the next deposit, and an idle time (t_{dw}) of 60 s was applied between two adjacent layers to cool down the walls by the atmosphere in the experimental room. The same set of processing parameters (a welding current of 70 A, a voltage of 18 V, and a traveling speed of 300 mm/min) was used to build the thin walls in these strategies.

(2) Studying the effect of the heat input on the shape and the microstructural evolution of built thin walls

In order to investigate the effects of the heat input on the shape and the microstructure evolution of thin walls, four thin-walled samples were built on a substrate according to the alternating direction deposition strategy (Fig. 3). The voltage U (V) and the travel speed v (mm/min) of the welding torch were kept constant at 18 V and 300 mm/min, respectively, for all samples. The welding current I (A) was varied from 50 to 110 A with an increment of 20 A, leading to a variation in the heat input Q. The heat input Q (J/mm) is determined by the following formula: $Q = \eta * 60 * U * I/v$, where η is the process efficiency and η is 0.8 for the gas metal arc welding process [34].

It is noted that the build of each thin wall was performed separately on the substrate. Namely, when the build of a thin wall was finished, the wall and the substrate were cooled down to room temperature. Thereafter, the build of the new wall on the substrate was started. The distance between two adjacent walls is about 20 mm. Therefore, it could be considered that the build of a wall does not significantly influence the other ones. Herein, the sample (S1) was first built with $I = 50$ (A), followed by S2, S3, and S4 with $I = 70$ (A), 90 (A), and 110 (A), respectively.

Table 1 Chemical elements of the ER70S-6 steel wire (in wt%) [33]

Element	C	Si	Mn	P	S	Ni	Cr	Mo	Cu	V
Standard	0.06–0.15	0.80–1.15	1.40–1.85	0.025	0.035	0.15	0.15	0.15	0.50	0.03
Typical	0.10	0.88	1.56	0.011	0.012	0.01	0.02	< 0.01	0.24	< 0.01

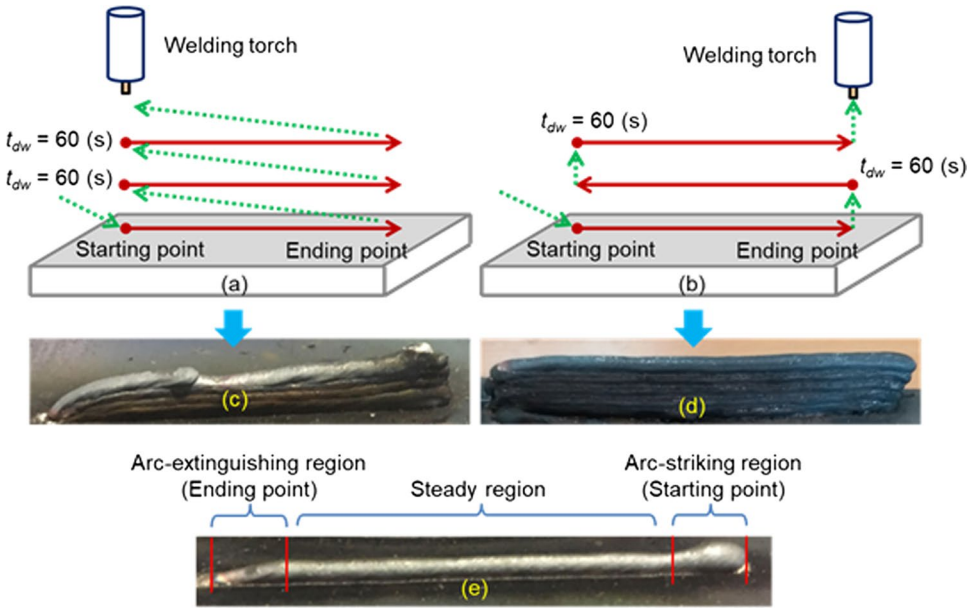

Fig. 2 Two deposition strategies for building thin walls (**a**, **b**), the corresponding shape of the walls built by two strategies (**c**, **d**), and the geometry of a single welding bead (**e**)

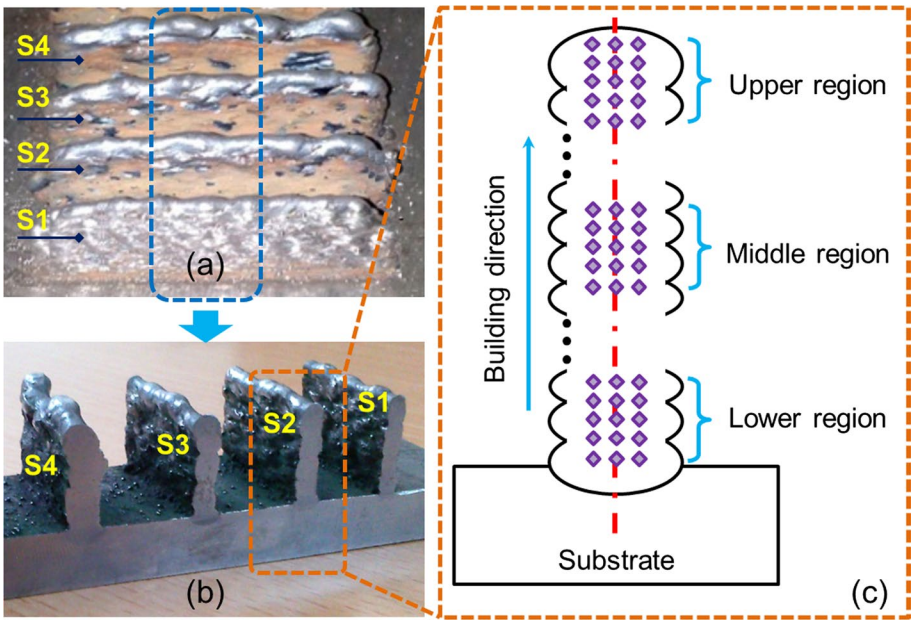

Fig. 3 **a** Four thin walls built on the substrate, **b** the specimen for observing the microstructures and measuring microhardness, and **c** a mapping of the microhardness measurement in three regions of each thin wall

The dimensions of the built walls, including the thickness and the height, were measured by a digital caliper of Mitutoyo with an accuracy of 0.02 mm (model 500-150-30). The length and the height of each built thin wall were about 80 mm and 18 mm, respectively. The thin-walled samples were also tested through X-ray computed tomography (CT) experiments to observe internal defects (Fig. 5).

To observe the microstructure and the hardness of as-built thin walls, a metallographic specimen was extracted from the thin walls by an EDM machine (Fig. 3b). The cross-sectional surface was then ground and polished. Finally, the surface was etched by using an etching solution of 5% Nital. The microstructures were analyzed by a microscope Axio Imager A2M of Carl Zeiss. The microstructures of the as-built thin wall were observed in three regions, namely the upper region, the middle region, and the lower region, as illustrated in Fig. 3c.

The hardness of thin walls was analyzed by a hardness testing machine (Vickers Future-Tech FV-110). In each hardness test, a load of 49.05 N and an idle time of 10 s were applied. The hardness measurement was also implemented in three regions where the microstructure was observed and in the center of the cross section of thin walls. The mapping for the hardness measurement is

depicted in Fig. 3c. In each region, the distance between two adjacent indentations is 0.5 mm. The hardness value is the average value of all indentations in each region.

The chemical composition of the as-built thin-walled material was also analyzed by a Thermo Scientific Spectrometer (ARL3460 OES). The percentage in weight of chemical elements of the as-built material is presented in Table 2. It was revealed that the chemical composition of the as-built thin-walled material falls within the same value range as that of the commercial ER70S-6 wire (Table 1).

(3) Observation on the tensile properties of the as-built thin-walled material

In order to observe the tensile properties of the as-built thin-walled material, a thin wall was built with the same set of processing parameters used in the first stage ($I = 70$ A, $U = 18$ V, and $v = 300$ mm/min), as shown in Fig. 4a. To prepare the tensile specimens, the surfaces of the wall were firstly machined to achieve the core of the welded material. Thereafter, two groups of tensile specimens (TShi and TSvi, with $i = 1$, 2, and 3) were cut by using a wire-cut EDM machine, and their dimensions are shown in Fig. 4b. The width and the gauge length of a tensile specimen are 6 mm and 20 mm, respectively. The tensile properties of the built thin-walled material were measured on a tensile tester (INSTRON 3369). The tensile tests were conducted at room temperature, and the speed of the cross head displacement was 1.2 mm/min.

3 Effects of deposition strategies on the shape of built thin walls

As shown in Fig. 2c, d, it was found that the alternating deposition direction enables the thin-walled sample with more regular height to be achieved. This phenomenon can be explained from the natural shape of a single welding layer. Normally, when the parameters of the welding process were not adjusted, the welding bead in the arc-striking region is higher than the steady region, and the bead height decreases toward the end of the welding bead (Fig. 2e) [12, 35]. In the alternating deposition direction strategy, the arc in the current welding layer was struck in the arc-extinguishing region and it was extinguished in the arc-striking region of the previous layer. Hence, the difference in terms of geometry between the arc-striking and the arc-extinguishing regions of the previous layer was effectively compensated in the current layer (Fig. 2d). On the other hand, in the same deposition direction strategy, the height of thin walls was significantly decreased from the arc-striking region to the arc-extinguishing region (Fig. 2c). Moreover, the difference in terms of height between the arc-striking region and the arc-extinguishing region increases when the number of deposited layers increases. A large variation in terms of height after certain deposited layers can also make the termination of the welding process and resulting geometrical defects (Fig. 2c).

Figure 4a reveals the thin wall built with the alternating deposition direction strategy. It is observed that the thickness of the wall is relatively regular, particularly in the middle

Table 2 Results of the chemical composition analysis on the GMAW-based AM-built thin wall (in wt%)

Element	C	Si	Mn	P	S	Ni	Cr	Mo	Cu	V
The as-built wall material	0.092	0.497	0.870	0.008	0.005	0.013	0.02	0.006	0.075	0.0098

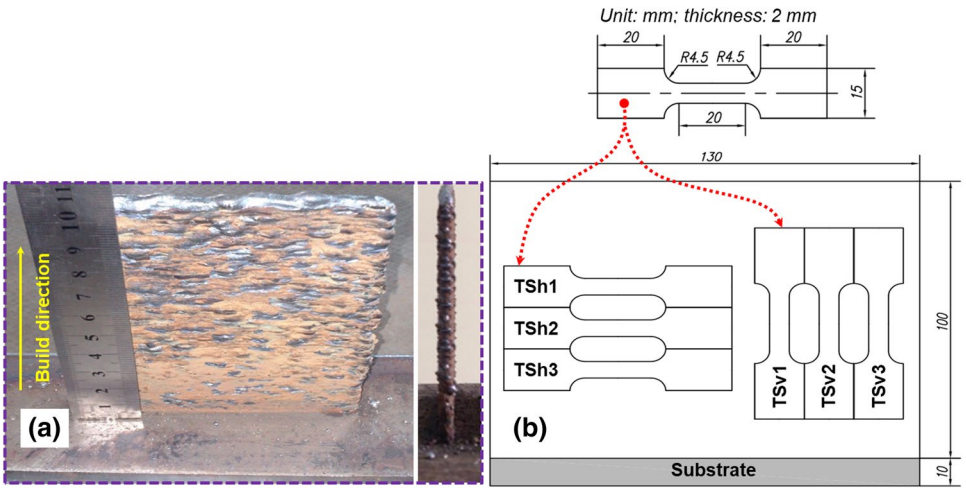

Fig. 4 GMAW-based AM-built thin wall (**a**) and the positions for cutting two groups of tensile specimens and the dimensions of all tensile specimens (**b**)

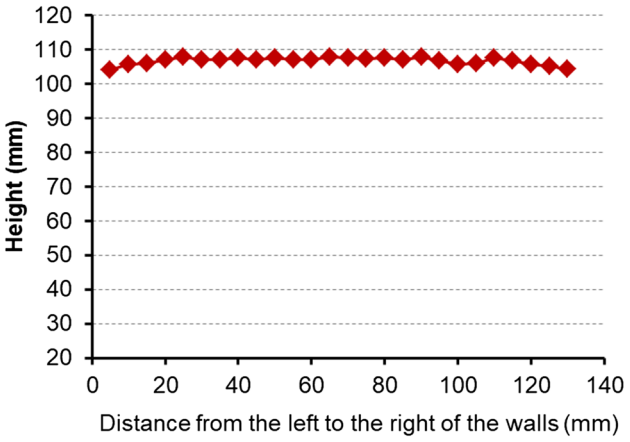

Fig. 5 Height variation of the wall built with the alternating deposition direction strategy

region. The average thickness of the thin wall is around 3.85 ± 0.14 mm. The height of the wall is also regular with an average value of 106.53 ± 1.02 mm. The height at the two ends of the wall is also lower than that of the middle region (Fig. 5). This is due to the fact that the heat dispassion condition in both end regions is worse than that of the middle region, and the fluidity of molten pool in both end regions is strong. Based on this result, in the following research stage, the alternating deposition direction strategy was chosen for building thin-walled samples.

4 Effects of the heat input on the microstructural evolution of built thin walls

4.1 Shape analysis

As shown in Fig. 3a, b, it was firstly found that the heat input has significant effects on the shape of the built thin walls. The thin walls (S1 and S2) built with lower heat inputs present a shape more stable than that of the samples built with higher heat inputs (S3 and S4). This phenomenon is due to the fact that when the heat input increased, the cooling rate of the whole thin-walled part decreased. At a certain height of the thin wall, the molten metal was also subsided due to an excessive heat input (e.g., S3 and S4 in Fig. 3b). However, the width of the walls built with low heat inputs is smaller than that of the walls built with high heat input [36]. The widths of the thin-walled samples S1, S2, S3, and S4 were 3.34 ± 0.10 mm, 3.74 ± 0.12 mm, 3.98 ± 0.18 mm, and 4.86 ± 0.13 mm, respectively. This is because the wire feed speed in the GMAW process increases with the increase in the welding current, resulting in an increase in the quantity of deposited material. Moreover, the increase in heat input leads to an increase in the welding bead width. That is why the wall S4 is the thickest, followed by S3, S2, and S1 (Fig. 3b).

4.2 Macro analysis

As shown in Fig. 3b, it can be observed that for all samples, there are no major defects (e.g., cracks) in both in the welded metal and the interface zones between the deposited wall and the substrate, indicating the compatibility of the consumable low-carbon steel wire for additive manufacturing. Furthermore, from the results of X-ray CT scan of all thin-walled samples (Fig. 6), no considerable pores or improper fusions between adjacent layers were found. These observations confirm that the GMAW-based AM allows thin walls to be built with high density, good bonding strength between layers, and without major defects.

4.3 Microstructure analysis

It was firstly observed that all thin-walled samples present the same microstructure characteristics without significant difference. These samples show a similar microstructure type in each region from the top to the bottom of built thin walls, i.e., the upper region, the middle region, and the lower region (Fig. 8). The heat input only has effects on the size of grains in each region of the built samples. Coarser grains were observed for the sample built with a higher heat input. For example, in the middle region, the average grain size of

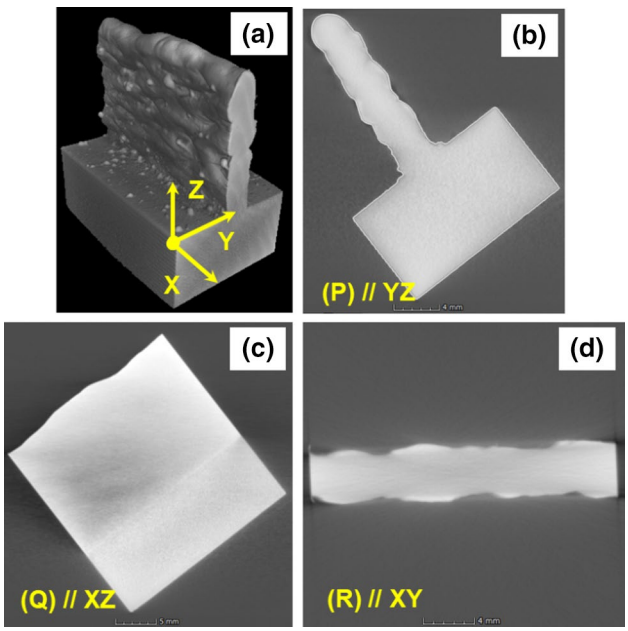

Fig. 6 X-ray computed tomography (CT) scan of a specimen extracted from S2 (**a**), and the results observed in three cross sections parallel to YZ (**b**), XZ (c), and XY (**d**) planes

the sample S4 which was built with the highest heat input was 13.30 ± 1.76 µm, whereas that of the sample S1 which was built with the lowest heat input was 11.2 ± 1.68 µm (Fig. 7). This is due to the fact that the solidification time was increased and the cooling rate was slowed down when a higher heat input was used to build the sample, thus resulting in coarser grains in microstructures.

To detail the microstructure of the as-built material in three regions of the wall, sample S2 was taken into account, which is representative for other samples. The microstructure in three regions of the as-built thin wall is shown in Fig. 8. The upper region shows lamellar structures composed of acicular and lamellar structures of ferrites with three grain types: Widmanstätten ferrite (α_w), allotriomorphic ferrite (α), and acicular ferrite (α_a) (Fig. 8a). This is due to the influence of continuous cooling by the natural air and the heat conduction toward the bottom of the built samples. In addition, the upper region features a high rate of cooling. This causes a transformation of microstructures from the primary austenite dendrites into typical Widmanstätten ferrites α_w.

On the other hand, the middle region reveals granular structures of ferrite with small regions of pearlite at grain boundaries (Fig. 8b). It was also observed that this region consists of two zones, namely the nonoverlapped zone (1) (Fig. 8b-1) and the overlapped zone (2) (Fig. 8b-2). The grains in zone (2) are moderately larger than the grains in zone (1). This is because of the heat effect of the molten pool that forms the current layer (i) on the previous layer ($i-1$). The layer ($i-1$) was reheated and partially remelted, resulting in the transformation in microstructure (e.g., the growth of grains) in the overlapped zone. Hence, a coarser grain size was observed in the overlapped zones.

The lower region consists of mixed lamellar and equiaxed grains of ferrites. The lamellar grains distribute and coexist with thin pearlites in the equiaxed grains of ferrites (Fig. 8c). In comparison with the grains in the middle region, the grain in this region is finer. Indeed, the lower region (including several first deposits) features a higher cooling rate, because it contacts the substrate. On the other hand, in the middle region, the heat accumulation increases with the number of layers [37]. Hence, the middle region presents a lower thermal gradient and a lower cooling rate [13].

Briefly, the heat input only has an effect on grain size, but it does not significantly influence the microstructure evolution of built thin walls. The built thin walls exhibited different microstructure types in different regions. The microstructure formation of the built samples is mainly due to the reheating and remelting effect of the deposition of successive layers and cooling cycles. The cooling in the calm air at room temperature is also similar for all samples. Hence, they reveal the same microstructure type in each region: the upper region, the middle region, and the lower region.

4.4 Microhardness analysis

As shown in Fig. 9, it was found that all the built samples reveal the same hardness evolution. The upper region of the samples reveals the hardest average hardness value, while the middle region shows the smallest average hardness value. This observation is in line with microstructures observed in Sect. 4.3 and the Hall–Petch relationship [38]. According to this relationship, the harness of materials is higher when the grain size in microstructure is finer.

Due to Widmanstätten structures (Fig. 8a), the microhardness of the upper region is higher than that of other regions. Because of the presence of lamellar structures (Fig. 8c), the lower region has the microhardness values higher than that of the middle region. Moreover, in each region, the sample built with lower heat input reveals relatively higher microhardness in each region. The reason is that a higher heat input leads to coarser grain size in microstructure of the built material. The microhardness of the samples S1, S2, S3, and S4 was in ranges of 162 ± 2.88 to 192 ± 4.30, 162 ± 3.51 to 191 ± 3.96, 160 ± 2.30 to 182 ± 2.30, and 157 ± 3.11 to 179 ± 3.16 (HV5), respectively.

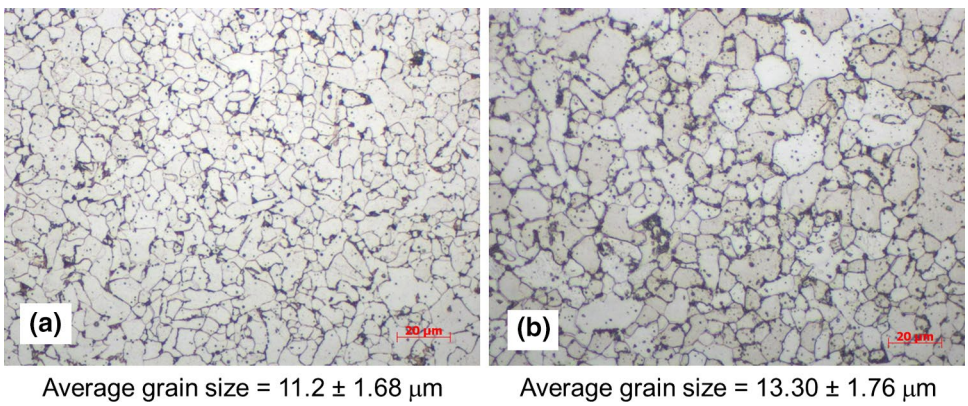

Fig. 7 Microstructure in the core of the same layer in the middle region between the samples S1 (**a**) and S4 (**b**)

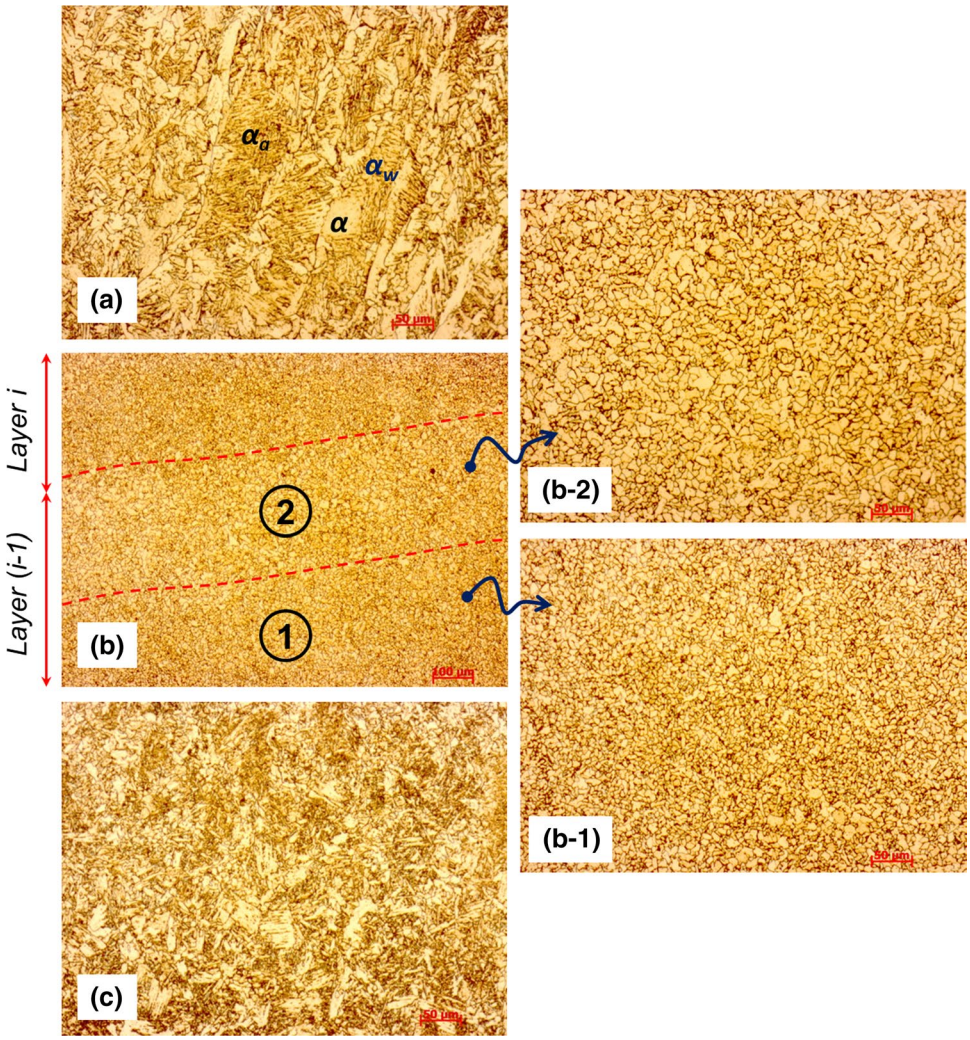

Fig. 8 Microstructures of built materials in the upper region (**a**), in the middle region with lower magnification (**b**), and in the lower region (**c**). The microstructure in the middle regions composed of nonoverlapped zone (1) (**b-1**) and overlapped zone (2) (**b-2**)

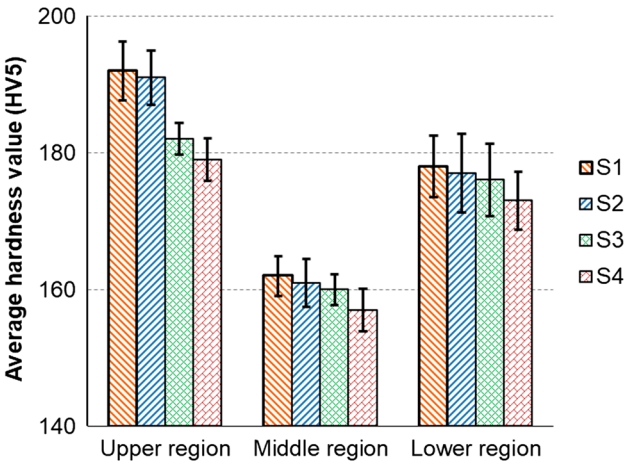

Fig. 9 Average value and standard deviation of hardness in each region

5 Tensile properties

Figure 10a presents the stress–strain curves of all tensile specimens in two groups. The strain–stress curves of all specimens present a typical behavior of low-carbon steels [39]. As revealed in Fig. 10b, it was found that the average values of UTS (ultimate tensile strength) and YS (yield strength) in the deposition direction (TSh*i*) were lower than those in the building direction (TSv*i*). The average values of YS and UTS of specimens TSv*i* are 362 ± 8 MPa and 479 ± 7 MPa, respectively, whereas the average values of YS and UTS of specimens TSh*i* are 320 ± 6 MPa and 429 ± 8 MPa. The deviation of YS/UTS between the depositing direction and the building direction might be caused by the anisotropy in the microstructure. In comparison with wrought A36 low-carbon steel (YS = 250 MPa and UTS = 400–550 MPa), which has similar chemical compositions as ER70S-6, the values of YS of all tensile specimens are higher, whereas their UTS values are in the range of UTS values of wrought A36 low-carbon steel [30].

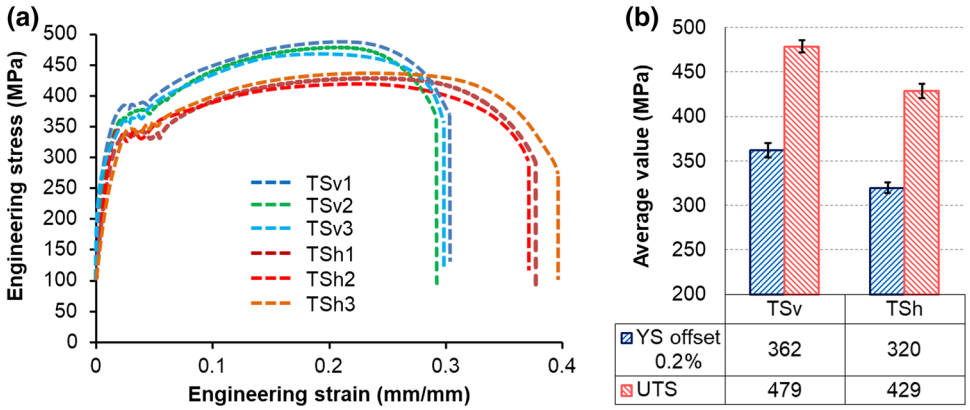

Fig. 10 Stress–strain curves of all tensile specimens (**a**) and the comparison between the average YS/UTS values of the vertical and horizontal tensile specimens (**b**)

6 Conclusions

In this paper, the effects of the deposition strategy and heat input in the GMAW-based additive manufacturing process on the shape and microstructure evolution of thin-walled components were firstly investigated. Thereafter, the most suitable deposition strategy and a set of process parameters were used to build a thin wall for tensile tests. The main results of this study can be summarized as follows:

- The alternating deposition strategy enables thin-walled components with more relatively regular height to be achieved.
- The GMAW-based AM process allows building thin-walled low-carbon components with a high density and without major defects such as cracks and improper fusions between adjacent layers.
- The variation in welding current leading to the variation in heat input levels has significant effects on the shape stability of built thin walls, but does not significantly influence the microstructure evolution and the microstructure type of the built thin walls. The increase in heat input only leads to coarser grains of the built thin wall and decrease in the hardness values.
- The microstructure of the built thin-walled material varies from the top to the bottom regions and can be distinguished in three regions, i.e., lamellar structures in the upper regions; granular structures of ferrites with small regions of pearlites at grain boundaries in the middle region; and equiaxed grains of ferrites in the lower region. This leads to the variation in hardness in different regions.
- There is a difference in terms of tensile properties between the depositing direction and the building direction, indicating the anisotropy in terms of mechanical properties of the GMAW-based AM-built thin-walled material.
- The mechanical properties of thin-walled low-carbon components built by the GMAW-based AM process are also comparable to those of wrought A36 low-carbon steel, which has similar chemical compositions compared to ER70S-6.

In future works, the surface quality and the thermal distortion of GMAW-based AM-built components will be studied. The surface quality and the thermal distortion are very important for the design and process planning stages. The generation of depositing paths for building multibead multilayer components and remanufacturing/repairing damaged components is also an interesting topic that needs to be addressed in future works.

Authors' contributions VTL proposed and designed the study. VTL, DSM, and QHH performed the experiments. VTL wrote the manuscript. All authors read, edited, and approved the final manuscript.

Funding This research is funded by Vietnam National Foundation for Science and Technology Development (NAFOSTED) under Grant Number 107.99-2019.18.

Availability of data and materials All data generated or analyzed during this study are included in this published article.

Compliance with ethical standards

Conflict of interest The authors declare that they have no competing interests.

References

1. Guo N, Leu M (2013) Additive manufacturing: technology, applications and research needs. Front Mech Eng 8:215–243. https://doi.org/10.1007/s11465-013-0248-8
2. Le VT, Paris H, Mandil G (2017) Environmental impact assessment of an innovative strategy based on an additive and subtractive manufacturing combination. J Clean Prod 164:508–523. https://doi.org/10.1016/j.jclepro.2017.06.204
3. Le VT, Paris H (2018) A life cycle assessment-based approach for evaluating the influence of total build height and batch size on the environmental performance of electron beam melting. Int J

Adv Manuf Technol 98:275–288. https://doi.org/10.1007/s00170-018-2264-7
4. Huang S, Liu P, Mokasdar A, Hou L (2013) Additive manufacturing and its societal impact: a literature review. Int J Adv Manuf Technol 67:1191–1203. https://doi.org/10.1007/s00170-012-4558-5
5. Arcam AB Corporation n.d. http://www.arcam.com/
6. Williams SW, Martina F, Addison AC, Ding J, Pardal G, Colegrove P (2016) Wire + Arc additive manufacturing. Mater Sci Technol 32:641–647. https://doi.org/10.1179/1743284715Y.0000000073
7. Ding D, Pan Z, Cuiuri D, Li H (2015) Wire-feed additive manufacturing of metal components: technologies, developments and future interests. Int J Adv Manuf Technol 81:465–481. https://doi.org/10.1007/s00170-015-7077-3
8. Buchanan C, Gardner L (2019) Metal 3D printing in construction: a review of methods, research, applications, opportunities and challenges. Eng Struct 180:332–348. https://doi.org/10.1016/j.engstruct.2018.11.045
9. Pires JN, Loureiro A, Bölmsjo G (2006) Welding robots: technology, system issues and application. Springer, London. https://doi.org/10.1007/1-84628-191-1
10. Zhang Z, Sun C, Xu X, Liu L (2018) Surface quality and forming characteristics of thin-wall aluminium alloy parts manufactured by laser assisted MIG arc additive manufacturing. Int J Light Mater Manuf 1:89–95. https://doi.org/10.1016/j.ijlmm.2018.03.005
11. Dinovitzer M, Chen X, Laliberte J, Huang X, Frei H (2019) Effect of wire and arc additive manufacturing (WAAM) process parameters on bead geometry and microstructure. Addit Manuf 26:138–146. https://doi.org/10.1016/j.addma.2018.12.013
12. Waqas A, Qin X, Xiong J, Wang H, Zheng C (2019) Optimization of process parameters to improve the effective area of deposition in GMAW-based additive manufacturing and its mechanical and microstructural analysis. Metals (Basel) 9:775. https://doi.org/10.3390/met9070775
13. Yang D, Wang G, Zhang G (2017) Thermal analysis for single-pass multi-layer GMAW based additive manufacturing using infrared thermography. J Mater Process Technol 244:215–224. https://doi.org/10.1016/j.jmatprotec.2017.01.024
14. Abe T, Sasahara H (2019) Layer geometry control for the fabrication of lattice structures by wire and arc additive manufacturing. Addit Manuf 28:639–648. https://doi.org/10.1016/j.addma.2019.06.010
15. Xiong J, Lei Y, Chen H, Zhang G (2017) Fabrication of inclined thin-walled parts in multi-layer single-pass GMAW-based additive manufacturing with flat position deposition. J Mater Process Technol 240:397–403. https://doi.org/10.1016/j.jmatprotec.2016.10.019
16. Xiong J, Li Y, Li R, Yin Z (2018) Influences of process parameters on surface roughness of multi-layer single-pass thin-walled parts in GMAW-based additive manufacturing. J Mater Process Technol 252:128–136. https://doi.org/10.1016/j.jmatprotec.2017.09.020
17. Hu Z, Qin X, Li Y, Yuan J, Wu Q (2019) Multi-bead overlapping model with varying cross-section profile for robotic GMAW-based additive manufacturing. J Intell Manuf. https://doi.org/10.1007/s10845-019-01501-z
18. Xiong J, Zhang G (2014) Adaptive control of deposited height in GMAW-based layer additive manufacturing. J Mater Process Technol 214:962–968. https://doi.org/10.1016/j.jmatprotec.2013.11.014
19. Yang D, He C, Zhang G (2016) Forming characteristics of thin-wall steel parts by double electrode GMAW based additive manufacturing. J Mater Process Technol 227:153–160. https://doi.org/10.1016/j.jmatprotec.2015.08.021
20. Zhao H, Zhang G, Yin Z, Wu L (2013) Effects of interpass idle time on thermal stresses in multipass multilayer weld-based rapid prototyping. J Manuf Sci Eng 135:011016. https://doi.org/10.1115/1.4023363
21. Ortega AG, Corona Galvan L, Salem M, Moussaoui K, Segonds S, Rouquette S et al (2019) Characterisation of 4043 aluminium alloy deposits obtained by wire and arc additive manufacturing using a cold metal transfer process. Sci Technol Weld Join 24:538–547. https://doi.org/10.1080/13621718.2018.1564986
22. Gokhale NP, Kala P, Sharma V (2019) Thin-walled metal deposition with GTAW welding-based additive manufacturing process. J Braz Soc Mech Sci Eng 41:569. https://doi.org/10.1007/s40430-019-2078-z
23. Silva CMA, Bragança IMF, Cabrita A, Quintino L, Martins PAF (2017) Formability of a wire arc deposited aluminium alloy. J Braz Soc Mech Sci Eng 39:4059–4068. https://doi.org/10.1007/s40430-017-0864-z
24. Derekar KS (2018) A review of wire arc additive manufacturing and advances in wire arc additive manufacturing of aluminium. Mater Sci Technol 34:895–916. https://doi.org/10.1080/02670836.2018.1455012
25. Wu B, Pan Z, Ding D, Cuiuri D, Li H, Xu J et al (2018) A review of the wire arc additive manufacturing of metals: properties, defects and quality improvement. J Manuf Process 35:127–139. https://doi.org/10.1016/j.jmapro.2018.08.001
26. Islam T, Rashed HMMA (2019) Classification and application of plain carbon steels, vol 2. Elsevier, Amsterdam. https://doi.org/10.1016/B978-0-12-803581-8.10268-1
27. Greer C, Nycz A, Noakes M, Richardson B, Post B, Kurfess T et al (2019) Introduction to the design rules for metal big area additive manufacturing. Addit Manuf 27:159–166. https://doi.org/10.1016/j.addma.2019.02.016
28. Laghi V, Palermo M, Gasparini G, Girelli VA, Trombetti T (2019) Experimental results for structural design of wire-and-arc additive manufactured stainless steel members. J Constr Steel Res. https://doi.org/10.1016/j.jcsr.2019.105858
29. MX3D. MX3D Bridge n.d. www.mx3d.com
30. Haden CV, Zeng G, Carter FM, Ruhl C, Krick BA, Harlow DG (2017) Wire and arc additive manufactured steel: tensile and wear properties. Addit Manuf 16:115–123. https://doi.org/10.1016/j.addma.2017.05.010
31. Rafieazad M, Ghaffari M, Vahedi Nemani A, Nasiri A (2019) Microstructural evolution and mechanical properties of a low-carbon low-alloy steel produced by wire arc additive manufacturing. Int J Adv Manuf Technol 105:2121–2134. https://doi.org/10.1007/s00170-019-04393-8
32. Lin Z, Goulas C, Ya W, Hermans MJM (2019) Microstructure and mechanical properties of medium carbon steel deposits obtained via wire and arc additive manufacturing using metal-cored wire. Metals (Basel). https://doi.org/10.3390/met9060673
33. Welding Handbook, KOBE STEEL, LTD. n.d
34. Quintino L, Liskevich O, Vilarinho L, Scotti A (2013) Heat input in full penetration welds in gas metal arc welding (GMAW). Int J Adv Manuf Technol 68:2833–2840. https://doi.org/10.1007/s00170-013-4862-8
35. Xiong J, Yin Z, Zhang W (2016) Forming appearance control of arc striking and extinguishing area in multi-layer single-pass GMAW-based additive manufacturing. Int J Adv Manuf Technol 87:579–586. https://doi.org/10.1007/s00170-016-8543-2
36. Wu Q, Ma Z, Chen G, Liu C, Ma D, Ma S (2017) Obtaining fine microstructure and unsupported overhangs by low heat input pulse arc additive manufacturing. J Manuf Process 27:198–206. https://doi.org/10.1016/j.jmapro.2017.05.004
37. Liberini M, Astarita A, Campatelli G, Scippa A, Montevecchi F, Venturini G et al (2017) Selection of optimal process parameters for wire arc additive manufacturing. Proc CIRP 62:470–474. https://doi.org/10.1016/j.procir.2016.06.124

38. Singh KK, Sangal S, Murty GS (2002) Hall-Petch behaviour of 316L austenitic stainless steel at room temperature. Mater Sci Technol 18:165–172. https://doi.org/10.1179/026708301125000384
39. Yan JB, Liew JYR, Zhang MH, Wang JY (2014) Mechanical properties of normal strength mild steel and high strength steel S690 in low temperature relevant to arctic environment. Mater Des 61:150–159. https://doi.org/10.1016/j.matdes.2014.04.057